Spatial and temporal evolution of a long term slow slip event: the 2006 Guerrero Slow Slip Event

Mathilde Radiguet, Fabrice Cotton, M. Vergnolle, Michel Campillo, Bernard Valette, V. Kostoglodov, Nathalie Cotte

Geophysical Journal International

Geophys. J. Int. (2011) **184,** 816–828 doi: 10.1111/j.1365-246X.2010.04866.x

Spatial and temporal evolution of a long term slow slip event: the 2006 Guerrero Slow Slip Event

M. Radiguet,[1] F. Cotton,[1] M. Vergnolle,[1,*] M. Campillo,[1] B. Valette,[2] V. Kostoglodov[3] and N. Cotte[1]

[1]*Laboratoire de Géophysique Interne et Tectonophysique, CNRS, Université Joseph Fourier, Maison des Géosciences, BP* 53, 38041 *Grenoble Cedex* 9, *France. E-mail: mathilde.radiguet@obs.ujf-grenoble.fr*

[2]*Laboratoire de Géophysique Interne et Tectonophysique, IRD:R157, CNRS, Université de Savoie, Campus Scientifique,* 73376 *Le Bourget-du-Lac Cedex, France*

[3]*Instituto de Geofísica, Universidad Nacional Autónoma de México, Mexico*

Accepted 2010 October 22. Received 2010 October 21; in original form 2010 June 4

SUMMARY

The Guerrero 2006 Slow Slip Event (SSE), Mexico, one of the world's largest observed SSEs, was recorded at 15 continuous GPS stations. This event provides the opportunity to analyse in detail the spatial and temporal evolution of slip at depth, and to constrain the characteristics of a large SSE. We perform an inversion in two steps. First, we invert the cumulative GPS displacements to retrieve the total slip amplitude. Second, we invert for the initiation time and duration of the slip, using a linearized least-squares inversion procedure and assuming a functional form for the slip function. Our results show that the slip is located on a patch of 300 km × 150 km (parallel and perpendicular to the coast, respectively), and extends from the bottom of the seismogenic zone to the transition zone. This slow slip event has an equivalent moment magnitude of 7.5. The maximum slip over a length scale of 25 km is 15 cm and the mean slip is 5.5 cm. Its lateral extension coincides with the segmentation of the subduction. Our inversion scheme allows us to analyse the spatial variability of the rise time, rupture velocity and slip function. We obtain a continuous image of the spatial and temporal variations of slip on the fault plane. The rupture initiated at a depth of 40 km (transition zone), in the western part of the Guerrero gap. The rupture then propagated from the western to the eastern part of the Guerrero segment with an average velocity of 0.8 km d^{-1}. Our results show that a slip dislocation pulse, characterized by a symmetric ramp function, can model the 2006 SSE. The rise time (local duration of slip) does not show large spatial variations and is equal to about 185 d. The local slip duration is compared to the total duration (11–12 months) of the event, suggesting a large interaction of a large part of the fault during the dynamic process. We find that our inverted slip model is well resolved on the shallow part of the fault and in the central section of the fault.

Key words: Time series analysis; Inverse theory; Seismic cycle; Transient deformation; Subduction zone processes.

1 INTRODUCTION

Recent geodetic observations allow detecting aseismic slow slip events in many subduction zones worldwide (Japan, Cascadia, Mexico, New Zealand, Costa Rica, Alaska; see Schwartz & Rokosky (2007) for a review). These SSEs show an important variability in terms of duration (from days to years), recorded surface displacements (a few millimetres to a few centimetres) and recurrence time. The mechanisms responsible for SSEs occurrences are still unclear. The SSEs are modelled as shear slip events occurring on the subduction plane and most studies show that the slip occurs below the locked, seismogenic section of the fault, in the transition zone between stick-slip and steady slip (Beroza & Ide 2009). The above observations raise significant questions as to the origin of slow slip events and their consequences for the seismic cycle.

Most SSEs studies only model the cumulative displacements, that is, they give a static image of the slip location on a fault plane and do not provide information on the evolution of slip with time (initiation, propagation velocity and termination). Analyses of slip propagation, however, are useful for understanding the physical mechanism responsible for SSEs occurrence and the possible

*Now at: Géoazur, Université de Nice Sophia-Antipolis, Centre National de la Recherche Scientifique, Observatoire de la côte d'Azur, France.

relation between SSEs and other associated phenomena such as non-volcanic tremors.

In the Guerrero subduction zone, Mexico, repeated large SSEs occurred in 1998, 2001–2002 and 2006 (e.g. Lowry *et al.* 2001; Kostoglodov *et al.* 2003; Larson *et al.* 2007; Vergnolle *et al.* 2010). A study of the SSEs in the Guerrero zone is then relevant for several reasons: (1) The Guerrero SSEs are large events, producing a few centimetres of surface displacements and lasting for several months. Therefore, the amplitude and duration of these events allow a detailed study of the spatial and temporal evolution of slip on the plate interface. (2) The short trench-to-coast distance and the 'flat slab' geometry of the subduction zone makes the Guerrero area well suited for studying SSEs: the slip occurs below the network of permanent GPS stations, which provides a reasonable resolution of the slip propagation on the plate interface. (3) Previous studies on this event show that slip probably intruded into the seismogenic zone (e.g. Larson *et al*. 2007; Vergnolle *et al.* 2010) hence shallower than what is observed for SSEs in most subduction zones. In this study, we perform an inversion of the GPS data and the associated resolution analysis to determine more precisely the extension of slip in the shallower portion of the subduction interface. (4) The direction of motion of the GPS stations during the SSE changes with time (Vergnolle *et al.* 2010). This suggests a complex spatio-temporal evolution of the slip on the plate interface, which we will characterize.

In this study, we perform the first analysis of the slip propagation on the subduction interface during the 2006 SSE in Mexico. We adopt a two-step inversion strategy (similar to the Hernandez *et al.* (1999) method for ordinary earthquakes). We first constrain the slip distribution and its uncertainty by inverting the GPS cumulative displacements and performing a detailed resolution analysis. In a second step, we determine the kinematic parameters. Our new SSE inversion scheme allows a kinematic study of the slip evolution using a limited number of parameters: the slip function is parametrized by the slip amplitude, the initiation time of slip and an accelerating and decelerating rise time which describe the duration and shape of slip at each fault point. Our inversion scheme allows us to assess the resolution of the obtained model parameters. We finally compare the characteristics of the 2006 Mexican SSE with other SSEs worldwide.

2 DATA AND TECTONIC CONTEXT

The Guerrero region is located on the southern Mexican coast along the boundary between the Cocos and North America plates. The geometry of the subducting slab has been evaluated by gravity anomaly modelling (Kostoglodov *et al.* 1996), hypocentres location (Pardo & Suarez 1995) and recently by receiver function analysis (Pérez-Campos *et al.* 2008; Kim *et al.* 2010). The subduction interface geometry we propose is based on the recent study by Pérez-Campos *et al.* (2008). The slab has a dip of ∼10° next to the trench (up to 40 km inland), then 20° up to 150 km inland and finally becomes subhorizontal 150 km inland, at a depth of ∼40 km. The Guerrero subduction segment includes the northwestern Guerrero gap (Fig. 1)

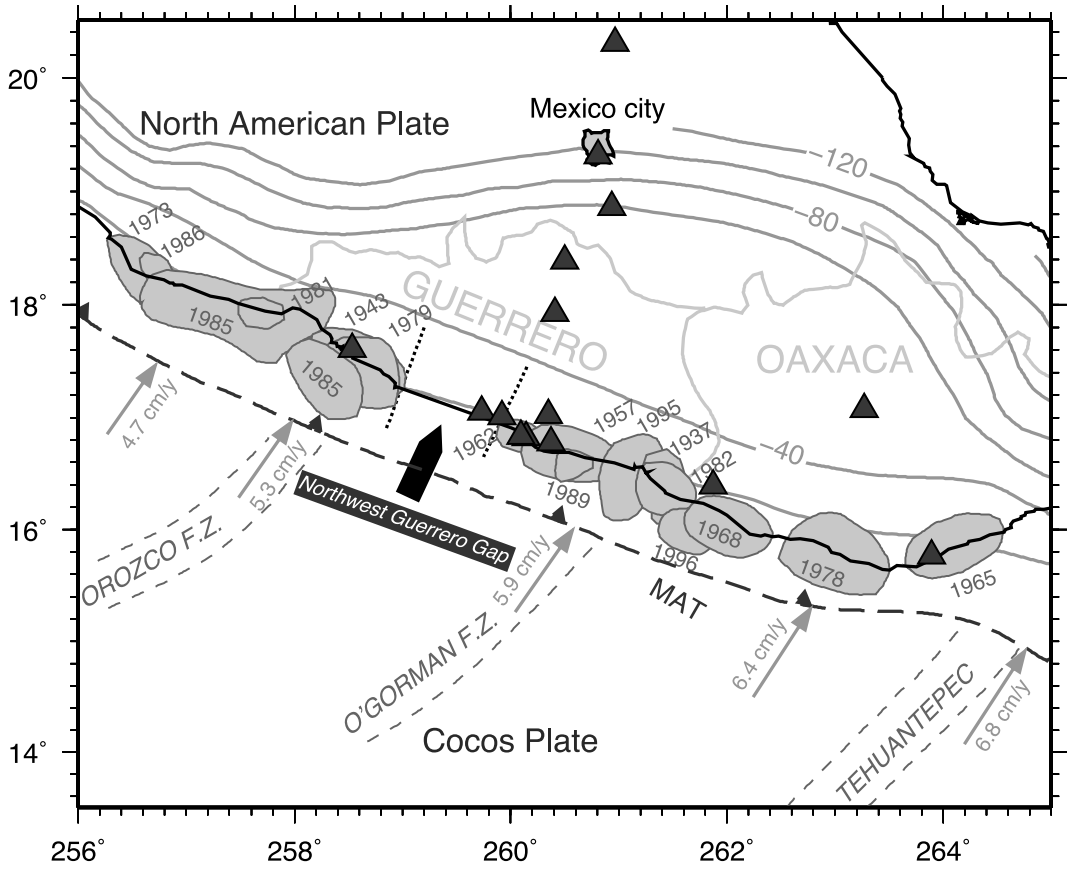

Figure 1. Seismotectonic map [after Kostoglodov *et al.* (2003)] and GPS station location (black triangles). The arrows indicate the direction and magnitude of NUVEL1A relative plate motion between the Cocos and North American Plate (DeMets *et al.* 1994). The grey patches represent the major earthquakes rupture zones. The thin grey lines represent the isodepth contour (in km) of the subducted oceanic slab (modified from Pardo & Suarez (1995) using the geometry proposed by Pérez-Campos *et al.* (2008)). MAT, Middle American Trench.

where no large subduction earthquake occurred since 1911. It is thus important to assess the seismic potential of this region because of its proximity to Mexico City.

The Guerrero 2006 SSE was recorded at 15 GPS stations of the Mexican permanent GPS network 'SSN-Sismologia-UNAM' (http://usuarios.geofisica.unam.mx/vladimir/gpsred/gpsred.html). The stations are located along the coast and on a transect perpendicular to the trench, between Acapulco and the north of Mexico City (Fig. 1). We use the GPS data recently re-processed by Vergnolle *et al.* (2010). The resulting 1997–2008 3-D GPS position time series in Guerrero show a noise reduction of ∼50 per cent with respect to previous studies.

We correct the GPS time series from the interevent steady-state motion by subtracting the linear trend from the period 2003–2005. The resulting time series (Fig. 2) thus show the deviation from the steady state motion during the 2006 SSE. We apply the median filter with a sliding window of 30 d and then we linearly interpolate the data to fill the data gaps. The data inversion is focused on the low frequency content of the GPS time series, so we apply a low pass filter on the smoothed and interpolated time series. The resulting time series (red traces in Fig. 2) are the data inverted in Section 4. They are composed of 64 points, covering a time period of 530 d (from 2006 January 1 to 2007 June 15) and the frequency band of the signal ranges from 0 to 6.9×10^{-7} Hz ($0.0596\ d^{-1}$). The inversion of GPS time series is done in the frequency domain.

We perform the inversion in two steps. First (Section 3), the cumulative GPS displacements are inverted to find the total slip distribution. In a second step (Section 4), we invert the GPS time series to retrieve the kinematic parameters, the final slip distribution being fixed to the value obtained in Section 3.

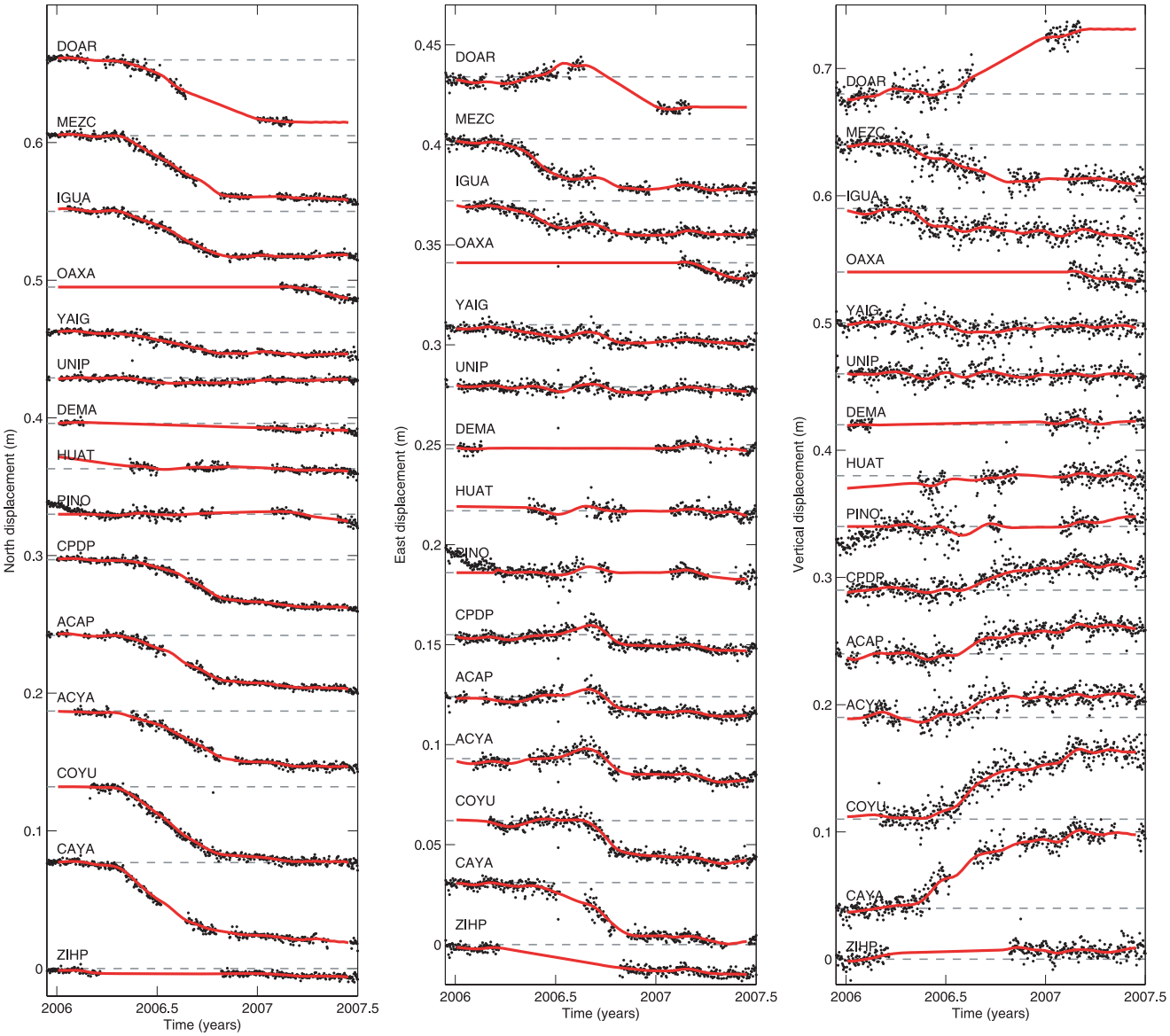

Figure 2. North, East and Vertical GPS time series for all analysed stations in this study (from Vergnolle *et al.* 2010). The black dots show the recorded positions corrected from the linear inter-SSE trend. Red lines are the filtered and interpolated data used in this study. Grey dashed line shows the zero displacement line for each station.

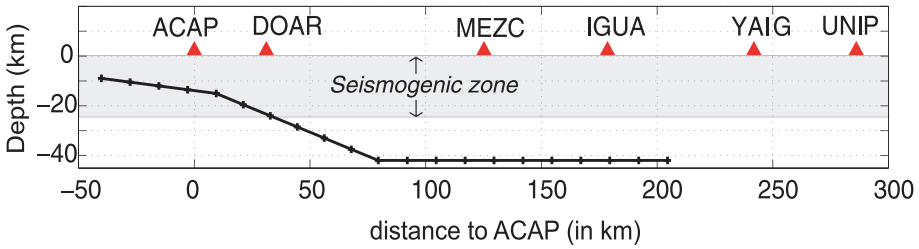

Figure 3. Geometry of the fault plane used in this study along a profile perpendicular to the trench (adapted from Pérez-Campos *et al.* (2008)). Red triangles are the GPS station located on the profile. Distances from the GPS site ACAP to the Trench is 66 km.

3 STATIC INVERSION (CUMULATIVE GPS DISPLACEMENTS)

3.1 Method and parametrization

We perform a static inversion of the cumulative GPS displacement to find the total slip distribution. The modelled fault plane is composed of 3 segments of varying dip angle (see cross-section in Fig. 3), and its total size is 468 km along strike (parallel to the coast) and 250 km along dip (perpendicular to the fault). The subfaults dimensions (12.5 km × 13 km) are rather small compared to the fault plane size. Doing so, we avoid imposing a strong *a priori* constraint on the slip location. A smooth solution is obtained by correlating nearby parameters. We invert for a fixed rake of 90° (pure thrust). Previous inversions for this SSE show that this choice is reasonable (Larson *et al.* 2007) and our results (see Sections 3.3 and 4.2) show that we can explain most of the data with this approximation. The transfer functions are calculated for a layered elastic half space, assuming the layered crustal model used by Hernandez *et al.* (2001).

The displacement at each GPS station is the linear sum of all subfaults contributions: $d = Gm$, where d are the observed displacements (3 components for each station), G is the matrix of transfer functions and m is the unknown vector of model parameters (slip on each subfault). We follow the least-squares formulation of Tarantola (2005) for linear problems. The cost function $S(m)$ is:

$$S(m) = \frac{1}{2}\left[(Gm-d)^t\ C_d^{-1}\ (Gm-d) + (m-m_0)^t\ C_m^{-1}\ (m-m_0)\right] \quad (1)$$

and the model expectation m is:

$$m = m_0 + C_m G^t \left(G C_m G^t + C_d\right)^{-1} (d - Gm), \quad (2)$$

where m_0 is the starting model, C_d and C_m are, respectively, the covariance matrix for data and model parameters. C_d is the diagonal matrix of the variances (σ_d^2) associated with the data errors. The standard deviations (σ_d) associated with North, East and Vertical component are two times the average standard deviations (95 per cent confidence level) for this component for all stations (2.1, 2.5 and 5.1 mm, respectively). We thus give the same weighting to all stations in the inversion, but a different weight depending on the component.

The model covariance matrix C_m is used to introduce correlation between nearby parameters, that is, spatial smoothing. The element (i, j) of C_m is given by the relation:

$$C_m(i, j) = \left(\sigma_m \frac{\lambda_0}{\lambda}\right)^2 \exp\left(-\frac{d(i, j)}{\lambda}\right), \quad (3)$$

where $d(i, j)$ is the distance between subfaults i and j. The parameters σ_m, λ and λ_0 are discussed below.

We use a decreasing exponential function $\exp(-\frac{d(i,j)}{\lambda})$ to introduce the correlation between nearby parameters (see Fig. 4a). Compared to the usually applied Gaussian function (Fig. 4b), the decreasing exponential stabilizes the solution at large distance, while allowing important variations in the slip amplitude for nearby subfaults. The model covariance matrix is weighted by a factor $(\sigma_m \frac{\lambda_0}{\lambda})^2$: σ_m is the *a priori* standard deviation of model parameters, fixed to 0.5 m, λ_0 is a scaling factor fixed to 10 km (about the size of a subfault) and λ is the correlation length, fixing the distance over which parameters are correlated. Note that as λ increases, more coefficients of the matrix C_m become non-null (more parameters are correlated). At the same time, the weighting factor $(\sigma_m \frac{\lambda_0}{\lambda})^2$ decreases as λ increases. The total weight of the matrix C_m thus remains constant for different values of λ. We tested several correlation lengths (from $\lambda = 5$ km (i.e. no correlation) up to $\lambda = 100$ km) and we used the L curve criterion (Hansen 1992) to select the optimum smoothing. It corresponds to the best compromise between the slip roughness and a low misfit to the data (Fig. 4c). The optimal correlation length of $\lambda = 35$ km was finally selected. The misfit to the data corresponds to the left hand term of the cost function (eq. 1).

In areas where the resolution is poor, the slip value resulting from the inversion remains close to the *a priori* slip value m_0 . To prevent spurious slip in poorly resolved areas, we took the zero slip model as a starting model. The slip distribution resulting from the inversion thus shows slip only in areas where it is necessary to explain the data.

3.2 Distribution of cumulative slip

The slip model resulting from the 2006 SSE (Fig. 4a) has an equivalent moment magnitude of 7.5. The slip distribution shows one major asperity of 300 km × 150 km (parallel and perpendicular to the trench respectively), with a maximum slip of 15 cm for the main asperity south of station MEZC (maximum slip averaged over 4 subfaults). The mean slip is 0.55 cm (calculated for subfaults in which the slip is >1 cm, see contour in Fig. 4a). No significant slip is observed in the shallowest, offshore subduction segment (from 20 to 70 km from the trench), at depths between 10 to 17 km. Deeper than 17 km, in the bottom part of the seismogenic zone, a significant slip (>5 cm) is observed. The slip extends up to 250 km from the trench.

Since no constraint was imposed on the positivity of the solution, some small and localized negative slip values appear. They reflect the uncertainties and errors associated with the inversion procedure (estimation of GPS cumulative displacements, fault plane geometry, 1-D earth model). The limited number of subfaults with negative slip values is an indication of the quality of the obtained solution. The data misfit (rms) between the N 3-D observed (d) and predicted (d_{mod}) surface displacements helps to evaluate the degree of agreement between the data and the model: $rms = \sqrt{\frac{1}{N}\sum_{i=1}^{N}(d^i_{\mathrm{mod}} - d^i)^2}$. The agreement between measured and modelled GPS cumulative displacements is very good: the rms data misfit is 1.2×10^{-3} m,

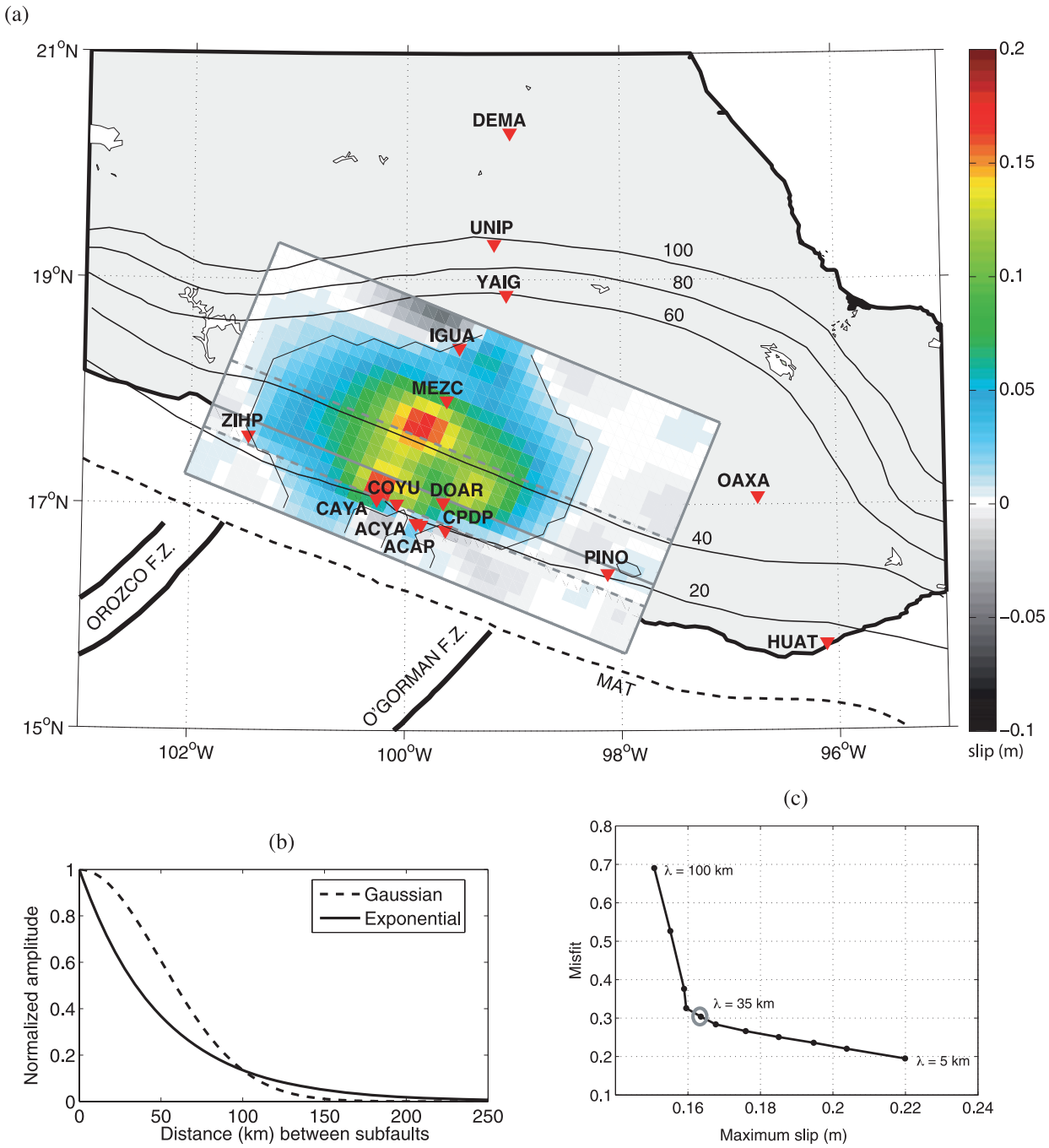

Figure 4. (a) Slip distribution resulting from the inversion of GPS cumulative displacements. The colours represent the slip amplitude. The contour line of slip >1 cm is represented. Red triangles show the GPS station locations and the thin black lines represent the isodepth contour (in km) of the subducted oceanic slab (modified from Pardo & Suarez (1995)). (b) Comparison of the Gaussian and decreasing exponential correlation functions. (c) Plot of misfit (left term of the cost function (eq. 1) as a function of maximum displacement (indication of the model roughness), for correlations lengths between 5 to 100 km (values tested: 5, 10, 15, 20, 25, 30, 35, 40, 50 75, 100 km). The best value is chosen for a correlation length of 35 km.

which is lower than two times the standard deviation σ_d for the three components.

3.3 Resolution analysis

Due to the uneven station distribution and to the decay of static displacement sensitivity with increasing slip depth, we expect the resolution of the inversion to be heterogeneous on the fault plane. We perform a resolution analysis to test which areas of the fault provide reliable information on the slip, in terms of amplitude and location.

The resolution matrix R satisfies the following equation (Tarantola & Valette 1982:

$$R = C_m G^t \left(G C_m G^t + C_d\right)^{-1} G. \quad (4)$$

If the resolution matrix equals the identity matrix, the estimated model is perfectly resolved. The farther the resolution operator is from the identity, the worse the resolution is.

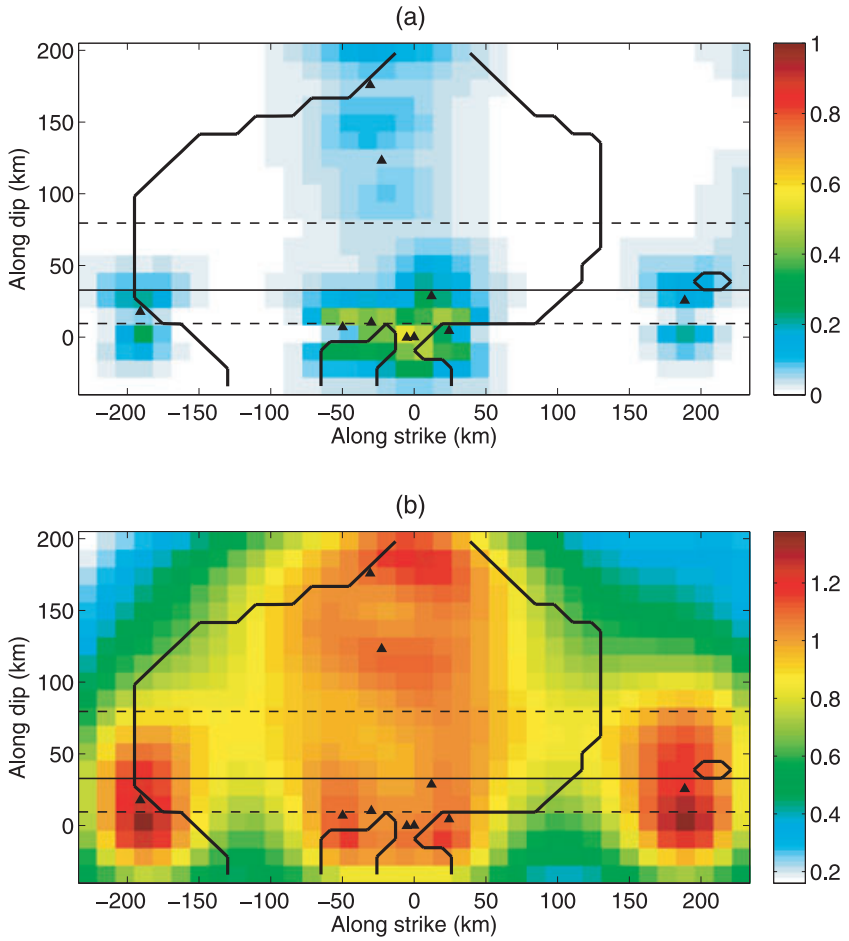

Figure 5. Resolution analysis. The surface projection of the fault plane is represented with the position of GPS stations (black triangles), the changes in dip (dashed lines) and the downdip limit of the seismogenic zone (thin black line). The contour plot of slip (slip >1 cm) is presented in thick black lines. Distances are in km from Acapulco. (a) Diagonal elements of the resolution matrix. (b) Restitution (sum of the rows of the resolution matrix).

Following Page *et al.* (2009), Fig. 5 gives different views of the resolution matrix. The diagonal elements (Fig. 5a) indicate how much slip of a particular subfault is correctly mapped to that subfault by the inversion. Fig. 5a shows that the resolution is quite low for individual subfaults. This result is not surprising: we have used a large number of subfaults (i.e. model parameters) in the inversion, even though the number of data (i.e. GPS stations) is limited. Using a large number of subfaults however avoids imposing *a priori* constraints on the slip location. This large number of parameters is balanced by the introduction of a correlation between neighbouring subfault parameters. It is then important to evaluate if slip of a particular subfault is correctly mapped onto neighbouring subfaults. This information is given by the off diagonal elements of the resolution matrix. The *i*th row of the resolution matrix indicates how the slip of the *i*th subfault has been mapped onto other subfaults. Summing the elements of the *i*th row of the resolution matrix (restitution index for the subfault *i*) indicates if the slip on the *i*th subfault has been completely mapped onto other subfaults (restitution index $\sim$1), or if some slip is not retrieved by the inversion (restitution index $<$1). The GPS stations are located mainly along the coast and on a line perpendicular to the fault. We thus expect the resolution to be high near the surface and on the middle of the fault plane, below the GPS stations. Fig. 5b shows the restitution index for all subfaults. In areas where the inversion shows slow slip (Fig. 4), the restitution index is higher than 0.8, which mean the slip is generally well retrieved by the inversion. The no slip region on the southeastern part on the fault (under the PINO station), is also well constrained. However, in the deeper corners of the fault plane, the restitution index is low ($<$0.5), which means the inversion is unable to resolve slip in these areas.

4 INVERSION OF GPS TIME SERIES

4.1 Inversion procedure

The second step of our inversion procedure is to invert the complete GPS time series, to find the spatial and temporal evolution of slip on the fault plane. We adapted the parametrized, frequency domain approach developed by Cotton & Campillo (1995) to the analysis of SSEs. We use a quasistatic approach: the transfer functions used in the inversion are static (calculated in a layered elastic half space) and the GPS time series are inverted in the frequency domain.

The fault parametrization is equivalent to the static case and the evolution of slip on each subfault is described by a slip function shown in Fig. 6. This slip function is parametrized by (1) the slip amplitude S_0, (2) the initiation time of slip t_0, (3) and (4) the accelerating t_1 and decelerating t_2 rise time, describing the duration of slip on each point. This formulation allows a kinematic study of slip evolution (rise time, rupture velocity and slip function can vary along space) using a limited number of parameters.

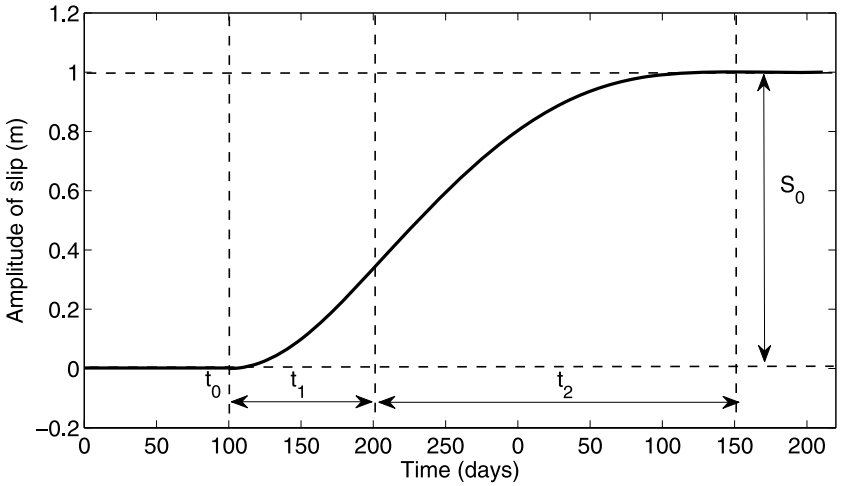

Figure 6. Parametrization of source time function (from Liu *et al.* (2006)). The source time function described the evolution of slip for each subfault as a function of 4 parameters: t_0 the initiation time of slip, t_1, the accelerating rise-time t_2, the decelerating rise-time and S_0 the amplitude of final slip. In this example, $t_0 = 50$ d, $t_1 = 50$ d, $t_2 = 125$ d and $S_0 = 1$ m.

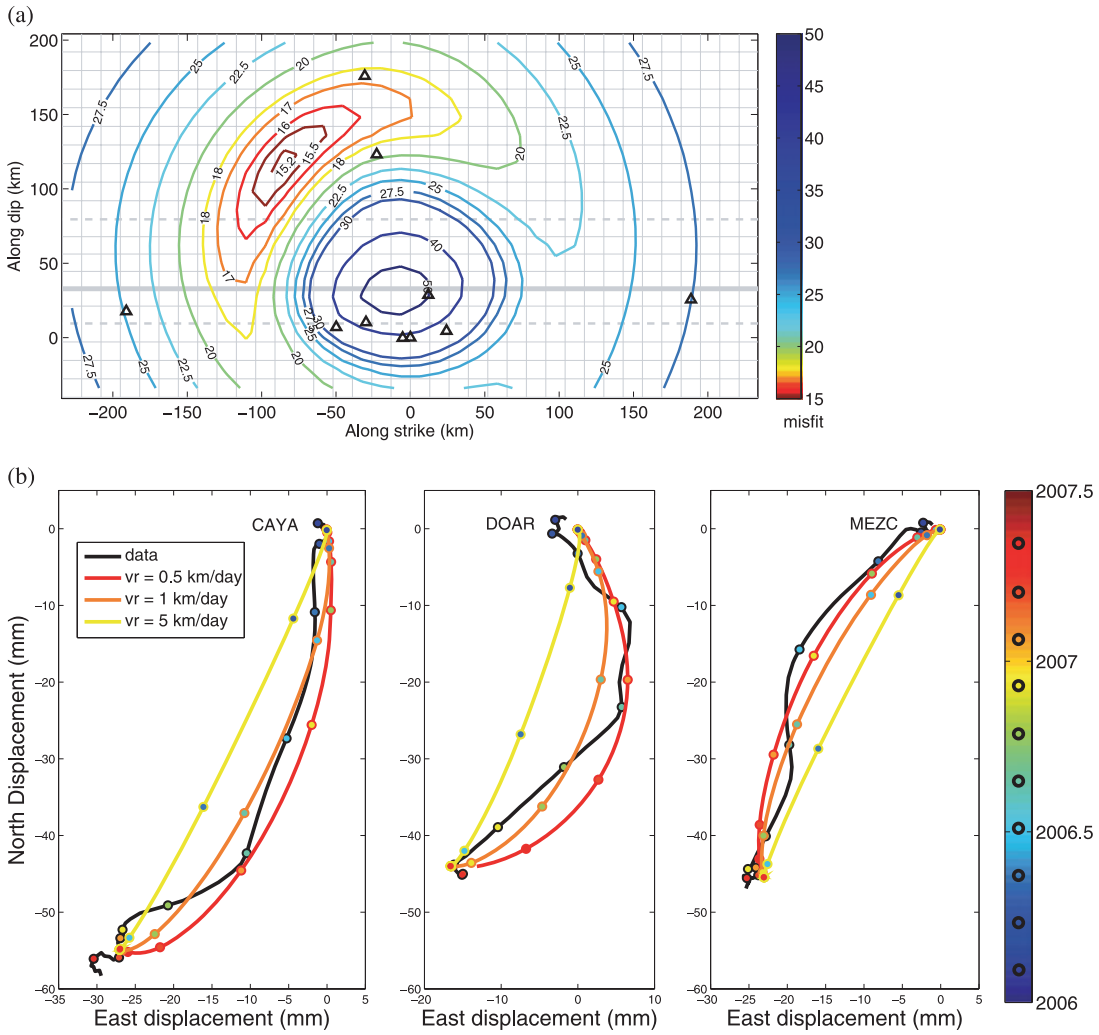

Figure 7. (a) Contour plot of misfit (left hand term of the cost function (eq. 1) for all initiation positions. ($v_r = 0.8$ km d^{-1}, $t_1 = t_2 = 185$ d). The surface projection of the fault plane is represented with the position of GPS stations (black triangles), the changes in dip (dashed lines) and the downdip limit of the seismogenic zone (thick line). Distances are in km from Acapulco. (b) Time evolution of northeast displacements at three stations. Black line is data, and coloured lines represent three different propagation velocities. The circles represent different times (see the coloured time scale on the right). The time period between each circle is 50 d. ($t_1 = t_2 = 185$ d, the initiation position corresponds to the lowest misfit in Fig.7a).

The inversion algorithm follows the linearized least-squares formulation of Tarantola & Valette (1982). The cost function is equivalent to the linear, static case (eq. (1)). The data vector d represents the analysed frequencies for each station and each component and the model vector m contains the 4 parameters describing the slip function for each subfault. The model expectation is given by the following relation (for the nth iteration):

$$m_{n+1} = m_n - \mu_n \left(G_n^t C_d^{-1} G_n + C_m^{-1}\right)^{-1} \left(G_n^t C_d^{-1} (d_n - d_{obs}) + C_m^{-1} (m_n - m_0)\right). \quad (5)$$

We apply the same weighting to different components as in the static case and down-weight by a factor of 10 the stations with important gaps in the GPS time series (DEMA, DOAR, HUAT, OAXA, PINO, ZIHP). These stations give information on the cumulative slip, but they cannot be used to constrain the propagation of slip. The slip amplitude is fixed by the static inversion. The parameters are correlated using the same correlation length of 35 km as in Section 3.

4.2 Forward modeling test and choice of initial inversion parameters

We first perform forward modelling tests assuming the slip distribution obtained in Section 3 and assuming a simple propagative model (constant velocity for slip propagation and constant rise time). Three parameters have been tested: the location of slip initiation, the propagation velocity (together, these parameters give t_{0i} for each subfault i) and the rise time (stating $t_1 = t_2$ for each subfault), giving a first-order evaluation of the characteristics of this event.

The results show that data are best modelled with a rise time t_1+t_2 of 185 d. The misfit as a function of slip initiation location is shown in Fig. 7a. It appears that the slip initiated on the western part of the fault. This is consistent with observations of the GPS time series, which show that the anomalous displacement was first observed at station CAYA, and then propagated south-eastward to stations COYU, ACYA, ACAP, DOAR (∼1 month later, 20 to 60 km away) and CPDP (2 months later, 75 km away) and north-eastward to inland stations MEZC and IGUA (∼1 month later, 120 to 170 km away) and finally to YAIG (Vergnolle *et al.* 2010).

Observation of the GPS time series indicates that the direction of horizontal displacements at stations located on the coast evolve from a southeastward displacement to a southwestward displacement, and that the change in direction occurs around July 2006. On the contrary, at the stations located inland, the horizontal displacement changes from southwest to south (Figs 7b and 10b). Fig. 7b shows the time evolution of horizontal displacements for 3 stations showing important variations in the direction of displacement with time. The data (black) are shown along with the predictions of three models characterized by different propagation velocities (0.5 km d^{-1}, 1 km d^{-1}, 5 km d^{-1}). These results show that the variations in the direction of displacement observed at the surface provide a strong constraint on the slip propagation velocity. A propagation velocity around 1 km d^{-1} is needed to explain the observed changes with the slip distribution presented in Fig. 4.

To refine the fit to the data, we then invert the GPS time series. We select 10 of the best models generated by the forward tests and use them as input models m_0 in the inversion. We thus produce 10 inversion results and the best one (lowest misfit) is presented in the next section. Note that the 10 inversion results are very similar.

5 RESULTS

The inversion confirms the results of the forward tests and provides information on regional variations. Fig. 8 shows the snapshots of slip propagation with time: the slip initiated in February 2006 in the western part of the Guerrero gap, 120 km southwest of station MEZC, on the flat portion of the slab interface, at a depth of 42 km. It propagated southeastward at a velocity of 0.8 km d^{-1} (on average). The maximum slip rates of 0.5 m yr^{-1} are observed in June–July 2006, in the centre of the modelled fault plane (below stations MEZC and CAYA, see Fig. 9b). The slip ends in January 2007, 250 km east of its initiation.

In the inversion, the slip propagation velocity, as well as the accelerating and decelerating rise time, are allowed to vary on the fault plane. However, the results of the inversion show that the data

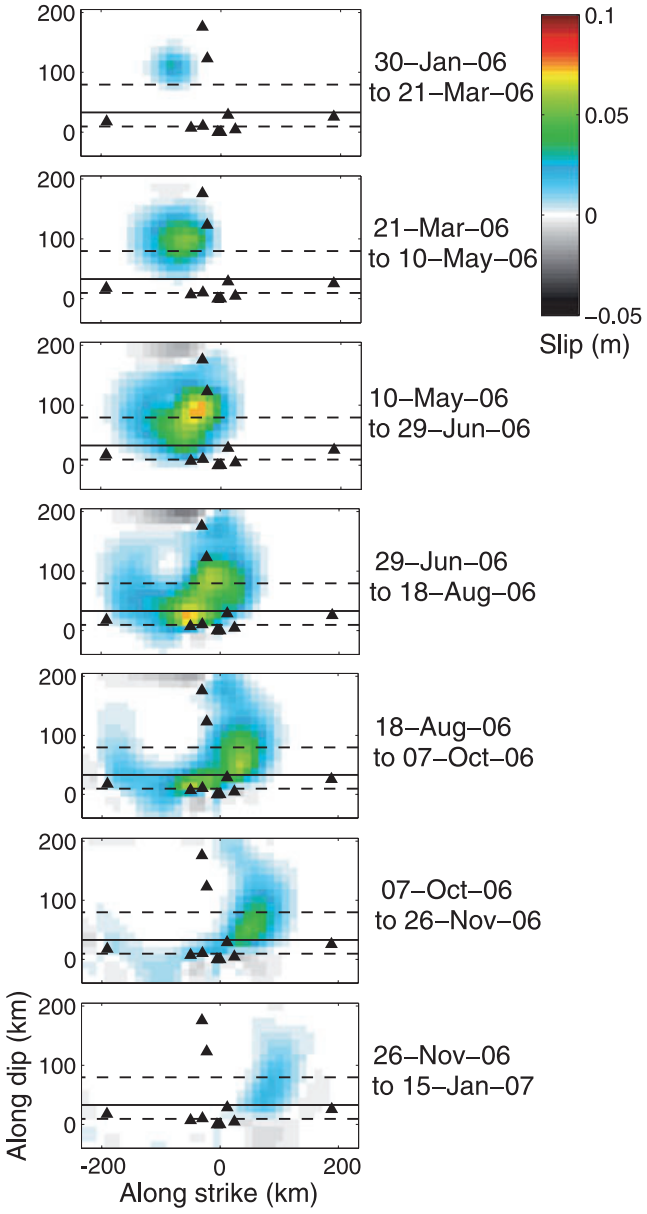

Figure 8. Snapshot of the slip propagation. Each plot covers a period of 50 d. The surface projection of the fault plane is represented with the position of GPS stations (black triangles), the changes in dip (dashed lines) and the downdip limit of the seismogenic zone (thin black line). Distances are in km from Acapulco.

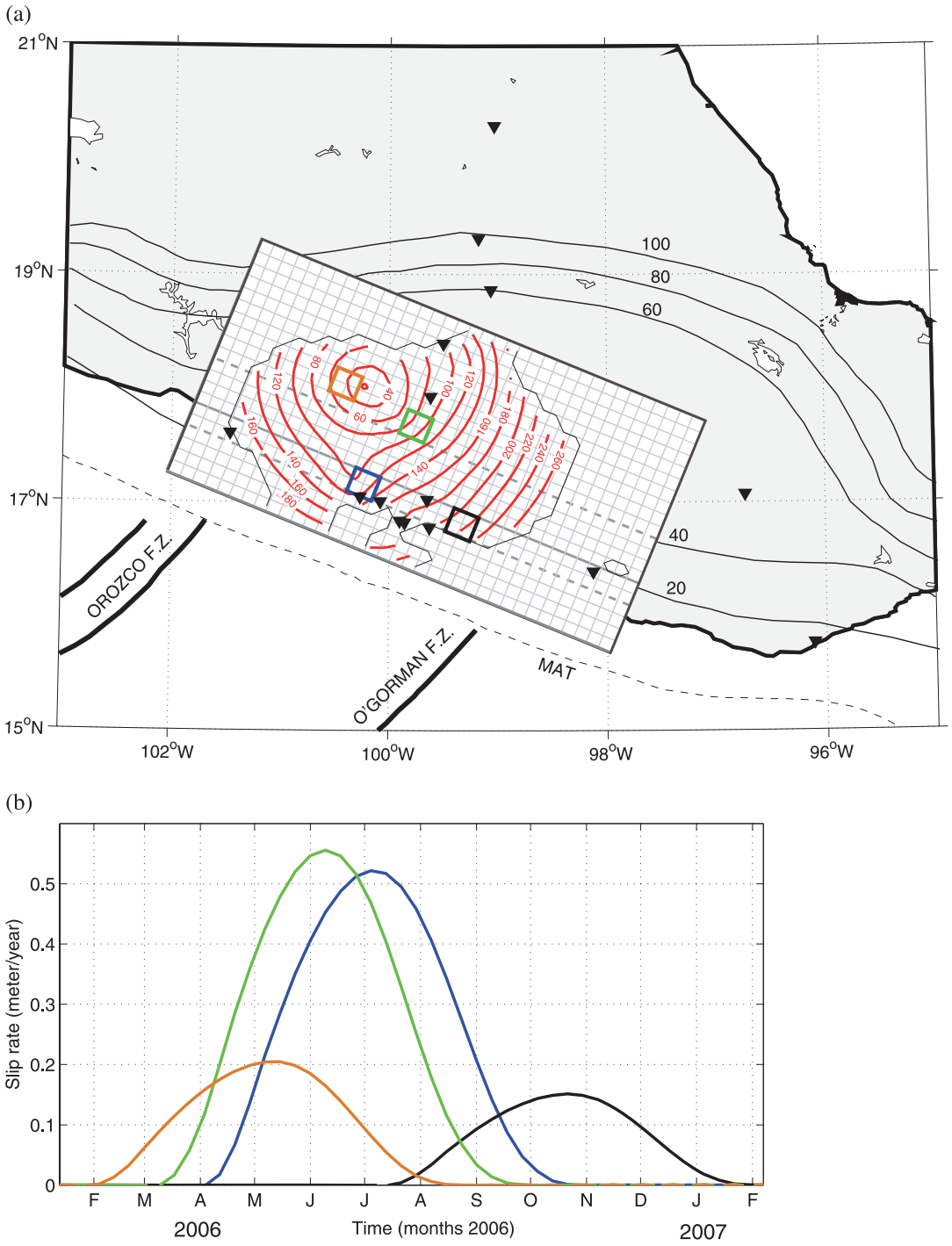

Figure 9. (a) Initiation time of slip along the fault. The red lines are the contour lines of initiation time (for slip >1 cm). Labels represent time in day from 2006, January 1. Coloured rectangles show areas for which the slip rate function (b) are plotted. (c) Fault plane view of rise time ($t_1 + t_2$), for slip >1 cm.

can be explained with a model in which the propagation velocity remains almost constant (Fig. 9a) around 0.8 km d^{-1}. Fig. 9c is a fault plane view of rise time (t_1+t_2). The rise time varies from 160 to 200 d (183 d in average). The rise time is longer near the coast (on the fault plane below stations CAYA, DOAR, ACAP) than on the north (below stations MEZC and IGUA). The duration of slip on the fault plane below the coast is thus longer than on the northern part of the fault plane. No significant difference appears between the accelerating t_1 and decelerating rise time t_2 (the slip rate functions shown in Fig. 9b for different location of the fault have indeed an almost symmetric shape). Our data set can be reasonably well fitted with simple slip functions, however our data coverage is probably too sparse to resolve complex slip functions and complex propagations velocities.

We obtain a good fit to the data (Figs 10a and b) with the model shown in Fig. 8. The average *rms* data misfit is 2.6 mm (2.20, 2.22 and 3.3 mm for the North, East and vertical components respectively). The model is able to accurately retrieve the

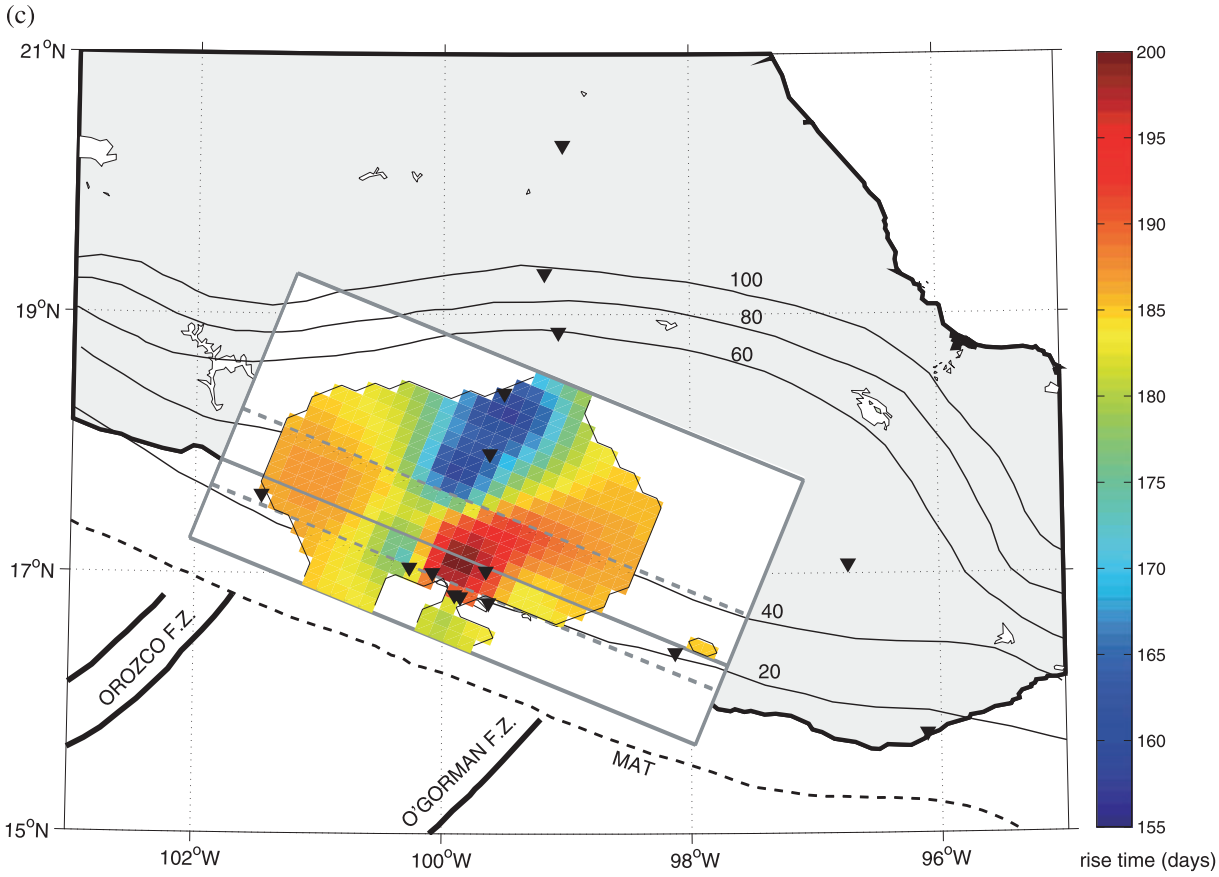

Figure 9. (*Continued.*)

observed displacement amplitudes, as well as most of the changes in the direction of displacement shown in Fig.10a. Our preferred model fits perfectly the sharp changes in slip direction for stations CAYA and COYU, and reasonably well for stations ACYA, ACAP, CPDP, DOAR and MEZC (Fig. 10a). Some details, however, are not retrieved correctly by the inversion. The limited coverage of the subduction area by the GPS stations does not allow the use of more complex models that may explain these small time scale variations.

5 DISCUSSION

5.1 Comparison between the 2006 Guerrero SSE and regular earthquakes

This spatio-temporal study of the large 2006 Guerrero SSE allows us to compare its kinematic characteristics with regular earthquakes.

The 2006 SSE propagated from the western to the eastern part of the Guerrero segment. We find that the lateral extension of the slip coincides with the segmentation of the subduction. Our propagative model shows that the slip initiates in the western part on the Guerrero segment, close to the Orozco fault zone, and propagates eastward toward the O'Gorman fault zone where it finally finishes (Figs 4 and 8). We thus suggest that termination of slip and the direction of propagation of this SSE are partially controlled by the position of potential slip barriers, similarly to what is observed for regular earthquakes (Manighetti *et al.* 2005, 2009; Wesnousky 2006). In the region where the 2006 SSE initiated, two moderate size earthquakes (Mw = 5.2) occurred in the time period corresponding to the slip initiation (on 2006 February 20 and 2006 March 20, Liu *et al.* 2007). The modelled slip evolution for the 2006 SSE also shows that the amount of slip on the interface is heterogeneous, and that the area of maximum slip is located some distance away from the area of slip initiation. This is also commonly observed for earthquakes (e.g. Manighetti *et al.* 2005): the hypocentre location is distinct from the main slip zone.

Our results show that the 2006 SSE recorded data can be described by a slip dislocation model characterized by a simple smooth ramp function. Such a functional form has been widely used to analyse regular earthquakes (e.g. Hernandez *et al.* 1999; Liu *et al.* 2006). The time duration of slip at a given point (rise time) is a key piece of information that helps to understand the rupture process. The rise time found for the Guerrero SSE is about half of the total duration. The duration of slip is then large with respect to the total duration of the rupture process, which means that there is a long distance interaction between points of the fault during the dynamic process (Fig. 9). This point differs from regular earthquakes: the rise time associated to a magnitude 7.0–7.5 regular earthquake (e.g. Landers 1992) being only 10–15 per cent of the total duration (Wald & Heaton 1994; Cotton & Campillo 1995).

The rupture area of the main asperity is about 45×10^3 km^2. The relationship between fault area and seismic moment (Kanamori & Anderson 1975) predicts a stress drop of 0.1–0.2 MPa which is 10 to 100 times less that regular earthquakes and of the order of stress drops observed for SSEs in the Cascadia subduction zone (Schmidt & Gao 2010).

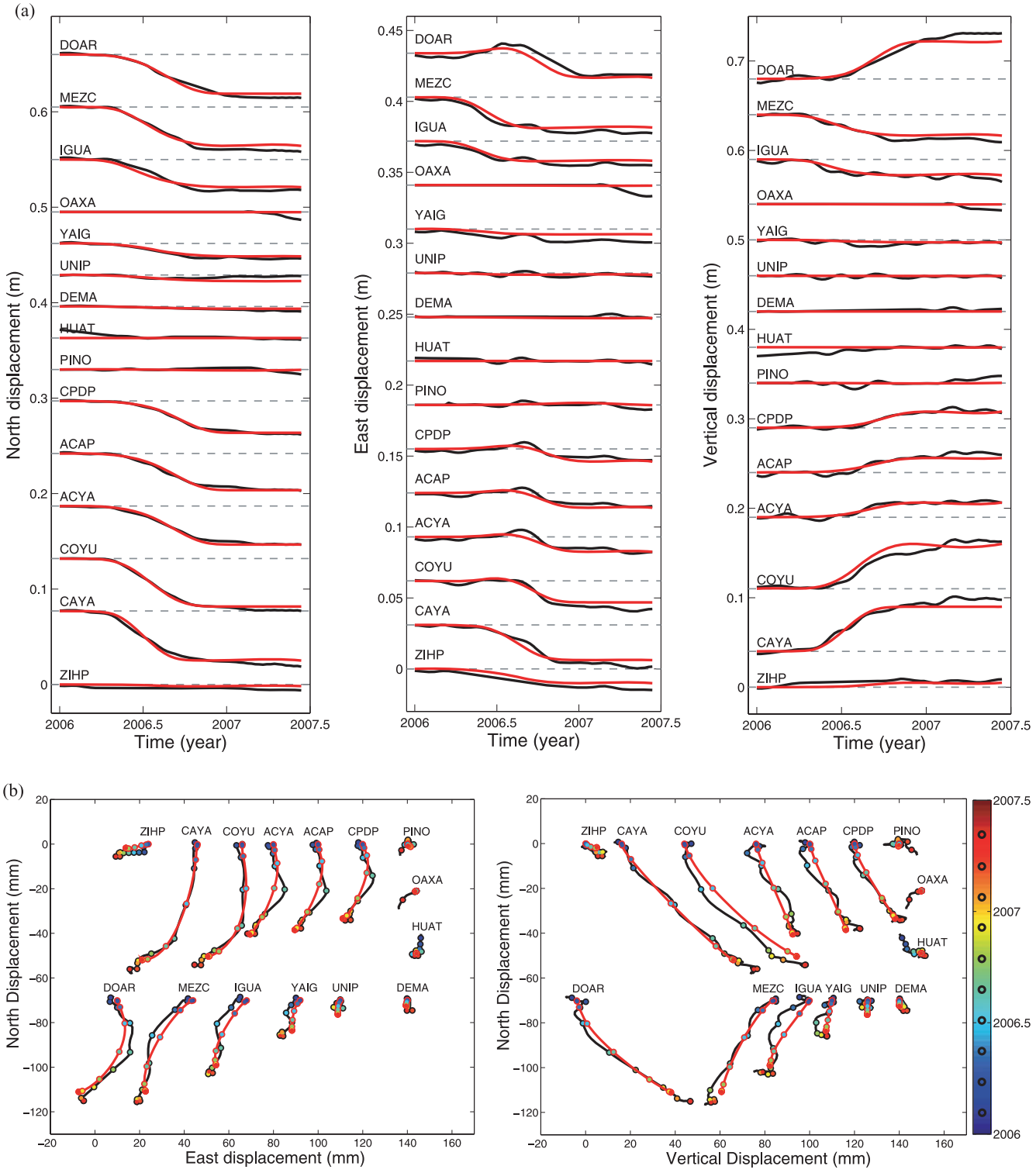

Figure 10. Time evolution of the displacement at each analysed station. Black lines represent the data, red lines the model. (a) Fit to north, east and vertical component. (b) Fit represented in 3-D. The circles represent different times (see the coloured time scale on the right). The time period between each circle is 50 d.

5.2 Comparison with others SSEs in the world

The duration of the 2006 Guerrero SSE (about 1 yr), is long compared to duration of SSEs in northern Cascadia (∼10 d, Dragert *et al.* 2004), in Bungo Channel and Nankai (a few days, Schwartz & Rokosky 2007). However, some long term SSEs have been identified in Tokai (duration over 5 yr, Miyazaki *et al.* 2006) and Bungo channel (duration about 1 yr, Miyazaki *et al.* 2003; Hirose & Obara 2005).

SSEs in Cascadia have equivalent moment magnitudes between 6.5 and 6.8, cumulative slip amplitude of 0.02 m and maximum

slip rate of 1 m yr^{-1} (Schmidt & Gao 2010). In long term SSEs in Japan, the equivalent moment magnitude reaches more than 7; the cumulative slip a few tens of centimetres and the maximum slip rate 0.13 m yr^{-1} in Tokai, 0.6 m yr^{-1} in the Bungo Channel. The characteristic of the Guerrero SSEs ($Mw \sim 7.5$, duration 1 yr, slip rate of 0.1–0.5 m yr^{-1}) is thus close to the long terms SSEs observed in Japan. Results from Schmidt and Gao (2010) suggest a proportionality between rise-time and slip such that slip rate of Cascadia SSEs is relatively constant during rupture. The varying resolution along strike complicates our analysis; however, our results do not suggest such dependency on the rise-time with the slip amplitude and therefore slip rates (Fig. 4, Figs 9a and b) are variable with a maximum value of 0.5 m yr^{-1}.

Detailed studies on slip propagation velocities are not available for most SSEs in the world, making the comparison between our results and other difficult. Most papers provide a 'migration velocity', which corresponds to the velocity at which the propagation of anomalous displacements is observed on the surface at the GPS receivers. This velocity is different from the velocity of slip propagation on the subduction plane. However, it has been noted that small SSEs propagate faster than large ones (Ide *et al.* 2007). For the 2006 SSE, we observe a propagation velocity of 0.8 km d^{-1}, which is effectively slower than the velocity observed for Cascadia events (3–10 km d^{-1}, Schmidt & Gao 2010).

6 CONCLUSIONS

Slow slip events are thought to represent source instabilities at the transition between velocity-weakening and velocity-strengthening portions of the plate (e.g. Liu & Rice 2005). GPS time series can constrain the temporal evolution of the 2006 Guerrero SSE, and our time-dependent inversion reveals the kinematic slip history of this Slow Slip Event. Our results show that the slip evolution during the SSE can be described with a rather simple smooth ramp. The rise-time of this slip is large with respect to the total duration of the rupture process, which means that there is an interaction between large parts of the fault during the dynamic process. This characteristic differs from regular earthquake properties. Variations in the direction of displacement observed at the surface provide a strong constraint on the slip propagation velocity. Our results show that a propagation velocity around 0.8 km d^{-1} explains the observations. This velocity is slower than the velocity observed for lower magnitude Cascadia events. Our results suggest that the extent and propagation of this SSE is controlled by the geometry of the subduction.

ACKNOWLEDGMENTS

The GPS network maintenance and data acquisition were supported by Mexico's PAPIIT IN102105, IN103808 and CONACYT 46064 grants. We are grateful to all the people who participated in the GPS network maintenance. We gratefully acknowledge the constructive reviews of the Associate Editor Y. Ben-Zion and two anonymous reviewers. This work has been supported by the French national programs Fluide-Faille-Flux (3F) from Institut National des Sciences de l'Univers/Centre National de Recherche Scientifique (INSU/CNRS) and by the French national research agency (Agence Nationale de la Recherche, ANR G-GAP RA0000C069). Fabrice Cotton and Michel Campillo benefited from Institut Universitaire de France support. We thanks other G-Gap participants (I. Manighetti, N. Shapiro, A. Walpersdorf, V. Cruz-Atienza) for their support and their stimulating discussions.

REFERENCES

Beroza, G. C. & Ide, S., 2009. Deep tremors and slow quakes, *Science,* **324,** 1025–1026.

Cotton, F. & Campillo, M., 1995. Frequency domain inversion of strong motions: application to the 1992 Landers earthquake, *J. geophys. Res.,* **100,** 3961–3975.

DeMets, C., Gordon, R.G., Argus, D.F. & Stein, S., 1994. Effect of recent revisions to the geomagnetic reversal time scale on estimates of current plate motions, *Geophys. Res. Lett.,* **21,** 2191–2194, doi:10.1029/94GL02118.

Dragert, H., Wang, K. & Rogers, G., 2004. Geodetic and seismic signatures of episodic tremor and slip in the northern Cascadia subduction zone, *Earth Planets Space,* **56,** 1143–1150.

Hansen, P. C., 1992. Analysis of discrete ill-posed problems by means of the L-curve, *SIAM Rev.,* **34,** 561–580.

Hernandez, B., Cotton, F. & Campillo, M., 1999. Contribution of radar interferometry to a two-step inversion of the kinematic process of the 1992 Landers earthquake, *J. geophys. Res.,* **104,** 13083–13099.

Hernandez, B. *et al*., 2001. Rupture history of September 30, 1999 intraplate earthquake of Oaxaca, Mexico (MW = 7.5) from inversion of strong-motion data, *Geophys. Res. Lett.,* **28,** 363–366.

Hirose, H. & Obara, K., 2005. Repeating short-and long-term slow slip events with deep tremor activity around the Bungo channel region, southwest Japan, *Earth Planets Space,* **57,** 961–972.

Ide, S., Beroza, G.C., Shelly, D.R. & Uchide T., 2007. A scaling law for slow earthquakes, *Nature,* **447,** 76–79.

Kanamori, H. & Anderson, D.L., 1975. Theoretical basis of some empirical relations in seismology, *Bull. seism. Soc. Am.,* **65,** 1073–1095.

Kim, Y., Clayton, R.W. & Jackson, J. M., 2010. Geometry and seismic properties of the subducting Cocos plate in central Mexico, *J. geophys. Res.,* **115**(B6), B06310.

Kostoglodov, V., Bandy, W., Dominguez, J. & Mena, M., 1996. Gravity and seismicity over the Guerrero seismic gap, Mexico. *Geophys. Res. Lett.,* **23,** 3385–3388.

Kostoglodov, V., Singh, S.K., Santiago, J.A., Franco, S.I., Larson, K.M., Lowry, A.R. & Bilham, R., 2003. A large silent earthquake in the Guerrero seismic gap, Mexico, *Geophys. Res. Lett.,* **30,** 1807–1811.

Larson, K.M., Kostoglodov, V., Shin'ichi, M. & Santiago, J.A., 2007. The 2006 aseismic slow slip event in Guerrero, Mexico: new results from GPS., *Geophys. Res. Lett.,* **34,** L13309, doi:10.1029/2007GL029912.

Liu, P., Custodio, S. & Archuleta, R.J., 2006. Kinematic inversion of the 2004 M 6.0 Parkfield earthquake including an approximation to site effects, *Bull. seism. Soc. Am.,* **96,** S143–S158.

Liu, Y. & Rice, J.R., 2005. Aseismic slip transients emerge spontaneously in three-dimensional rate and state modeling of subduction earthquake sequences, *J. geophys. Res,* **110,** B08307, doi:10.1029/2004JB003424.

Liu, Y., Rice, J.R. & Larson, K.M., 2007. Seismicity variations associated with aseismic transients in Guerrero, Mexico, 1995–2006, *Earth planet. Sci. Lett.,* **262,** 493–504.

Lowry, A., Larson, K., Kostoglodov, V. & Bilham, R., 2001. Transient slip on the subduction interface in Guerrero, southern Mexico, *Geophys. Res. Lett.,* **28,** 3753–3756.

Manighetti, I., Campillo, M., Sammis, C., Mai, P. & King, G., 2005. Evidence for self-similar, triangular slip distributions on earthquakes: implications for earthquake and fault mechanics, *J. geophys. Res.,* **110,** B05302, doi:10.1029/2004JB00317.

Manighetti, I., Zigone, D., Campillo, M. & Cotton, F., 2009. Self-similarity of the largest-scale segmentation of the faults: implications for earthquake behavior, *Earth planet. Sci. Lett.,* **288,** 370–381.

Miyazaki, S., McGuire, J. & Segall, P., 2003. A transient subduction zone slip episode in southwest Japan observed by the nationwide GPS array, *J. geophys. Res.,* **108,** 2087.

Miyazaki, S., Segall, P., McGuire, J.J., Kato, T. & Hatanaka, Y., 2006. Spatial and temporal evolution of stress and slip rate during the 2000 Tokai slow earthquake. *J. geophys. Res,* **111,** 1997–2002.

Page, M.T., Custódio, S., Archuleta, R.J. & Carlson, J., 2009. Constraining earthquake source inversions with GPS Data 1: resolution based removal of artifacts., *J. geophys. Res.,* **114,** B01314, doi:10.1029/2007JB00544.

Pardo, M. & Suarez, G., 1995. Shape of the subducted Rivera and Cocos plates in southern Mexico: seismic and tectonic implications, *J. geophys. Res.,* **100,** 12357–12373.

Pérez-Campos, X. *et al*., 2008. Horizontal subduction and truncation of the Cocos Plate beneath central Mexico, *Geophys. Res. Lett.,* **35,** L18303, doi:10.1029/2008GL035127.

Schmidt, D. & Gao, H., 2010. Source parameters and time-dependent slip distributions of slow slip events on the Cascadia subduction zone from 1998 to 2008, *J. geophys. Res.,* **115,** B00A18, doi:10.1029/2008JB006045.

Schwartz, S.Y. & Rokosky, J.M., 2007. Slow slip events and seismic tremor at circum-Pacific subduction zones, *Rev. Geophys.,* **45,** RG3004, doi:10.1029/2006RG00020.

Tarantola, A. & Valette, B., 1982. Generalized non-linear inverse problems solved using the least square criterion, *Rev. Geophys. Space Phys.,* **20,** 219–232.

Tarantola, A. 2005. Inverse problem theory and methods for model parameter estimation, *Society for Industrial and Applied Mathematics (SIAM), Philadelphia.*

Vergnolle, M., Walpersdorf, A., Kostoglodov, V., Tregoning, P., Santiago, J.A., Cotte, N. & Franco, S.I., 2010,. Slow slip events in Mexico revised from the processing of 11 year GPS observations, *J. geophys. Res*., **115,** B08403, doi:10.1029/2009JB006852.

Wald, D.J. & Heaton, T.H., 1994. Spatial and temporal distribution of slip for the 1992 Landers, California, earthquake, *Bull. seism. Soc. Am.,* **84,** 668–691.

Wesnousky, S.G., 2006. Predicting the endpoints of earthquake ruptures, *Nature,* **444,** 358–360.